Responses to reviews

"Influence of Secondary Ice Production on cloud and rain properties: Analysis of the HYMEX IOP7a Heavy Precipitation Event"

by Grzegorczyk., P, et al.

10 June, 2025

We thank the two reviewers, whose comments have led to significant improvements of our manuscript. Our point-to-point answers to each comment are highlighted in red here below. The manuscript modifications will be visible in the manuscript thanks to the Change Tracking option. Nevertheless, we also copied below the modified sentences of the manuscript in gray and italic.

Reviewer #1:

The authors of this manuscript examined the impact of SIP processes, including Hallett-Mossop, drop shattering during freezing and ice-ice collision breakup, in a real case model simulation with a 3D bin microphysics scheme (DESCAM). It is found that including SIP, the model produced slightly higher TWC, and higher ice number concentration for T>-20°C. Adding SIP improvement of the agreement between simulation results and the observations for ice number concentration, TWC, drop number fraction (> 300 microns) as well as size distributions for both ice and liquid at the altitudes where SIP is active (5-6 km). The contributions of each SIP process, based on the current parameterizations, at different altitudes were quantified. Simulated precipitation amounts from both SIP and noSIP runs are generally lower than the observations. The SIP run produced lower precipitation amount, more smaller drops and less larger drops compared to noSIP run. Adding SIP in the simulation will also modify the mass distribution of hydrometeors with more mass for the smaller particle/drop sizes.

The manuscript is well written. The experiment and the results are well presented. The scope of the study aligns well with the focus of the journal. I therefore recommend the publication of this manuscript after addressing the following comments.

General:

Fig 2a: what's the range of the invalid range of radar signal just above and below the aircraft. I didn't see any data being masked out in the near-aircraft region.

In Fig 2, there is around +/- 300 m of invalid radar signal above and below the aircraft. Within this range, values are therefore interpolated. It is now mentioned in the caption of Fig. 2 as *"RASTA W-band radar reflectivity observation and aircraft altitude (Reflectivity values within ± 300 m of the aircraft are interpolated)."*

L139: please also add descriptions of the temperature range and dependency for H-M process.

Details about the HM process temperature are now provided (see line 144 or line 148 of diff pdf): *"The first SIP process considered in DESCAM is the Hallett-Mossop process (HM) which is activated between -3° C to -8°C. It is temperature dependent within this temperature range, reaching a maximum of 350 fragments per mg of rime produced at -5°C (Hallett and Mossop, 1974). This temperature dependency is based on Eq. 72 of Cotton et al. (1986). More details about HM are presented in Section A1 of Appendix A. "*

Furthermore, a detailed description of the parameterization of HM (as well as BRK and DS processes) has been added in appendix (available at the end of the document) regarding reviewer #2 comments.

L176-177: How was the averaging of the model results performed? Only for in-cloud region or the entire zone highlighted in Fig. 1b? Or is there any selection of the areas close to the aircraft track?

Only in-cloud regions were selected. We prefer to average the model on a large area where the aircraft sampled the cloud system (which is indicated by dashed red line in Fig 1b) and by considering TWC and w values in the range that was observed by the aircraft. This ensures to select more numerous points and to the be more statistically significant.

Regarding the possibility of selecting an area close to the aircraft track, as the model cannot perfectly reproduce the sampled cloud system, the aircraft may pass through specific cloud regions (e.g. stratiform cloud system), whereas the model may provide a different condition at the position and time or the aircraft (i.e. strong convective area or even no clouds). We tried to clarify that in section 3.2 (see line 179 or line 187 of diff pdf) with "*Contrary to selecting grid points near the aircraft track, this method ensures that the model closely matches the observed conditions, excluding strong convective regions where no measurements were made for safety reasons. It also allows the selection of much more data points in the model, leading to a better statistical significance, and improving the robustness of the comparison.*

Fig. 3: should the shade area of noSIP simulation be added as well?

Good point, we updated this figure, thank you.

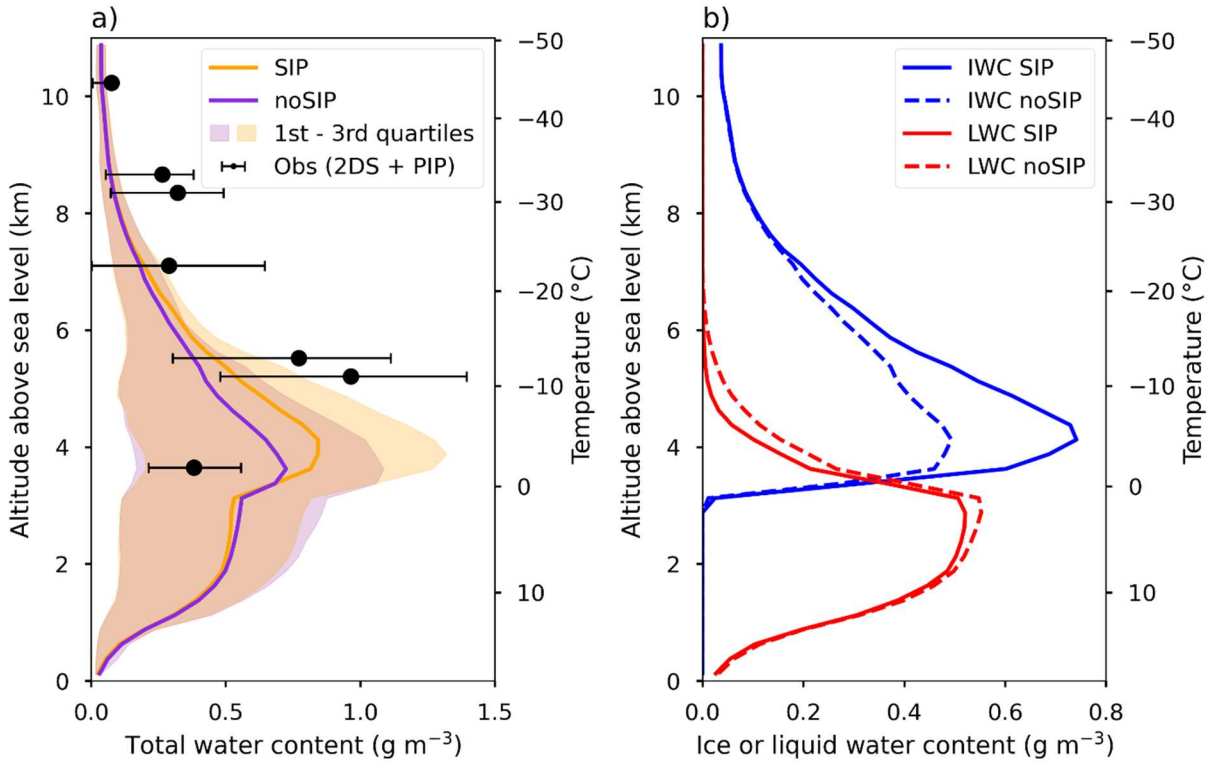

L200: however, there are values at ~7.5 and 9 km though. One is closer to noSIP, another one much higher than both simulations.

Yes that is true, but as we mention in the previous sentence, "At higher altitudes, it is important to note that in two cases (at 8.5 km and 10 km), the observed drop fraction is zero, and that these points are therefore not represented in Fig. 4a."

It is therefore difficult to say which simulation provides the best agreement with observations regarding the variability of the 4 drop fraction points in Fig 4a for T < -20°C (two equal to 0 and 2 others at 0.2 and 0.02 %). The sentence line 200 that you mention, as well the previous one are updated *(*see line 219 or line 227 of diff pdf) with *"However, with only four data points that vary significantly, it remains difficult to determine which simulation better matches the observations near the cloud top. Additional observations are needed to better evaluate the liquid and ice partitioning in DESCAM depending on environmental factors such as the convective and stratiform cloud regions observed after and before 08:15 UTC."*

196-198: good point.

Thank you

Fig. 4: the aircraft observed different altitudes/regions. Some flight legs were continuously in-cloud, and some others sampled updraft like towers especially at higher altitudes. These clouds might be quite different in terms of microphysical properties. Using a single average model profile for the comparison with the aircraft data might miss a lot of detailed information. In the comparison here, I would suggest exploring to have more categorized comparisons depending on different altitudes & cloud types (continued, updrafts, etc.) which might help to better understand the differences between simulations and observations.

Yes, you are right, it could be interesting to distinguish datapoints in some regions of different convection intensity. We tried to separate the observations into two periods: before and after 8:15 UTC which corresponds to the stratiform and convective phases of the cloud respectively. The separation of these two phases is consistent with the radar reflectivity as well as morphology of ice particles (see Fig 1a and c).

In the model, we determine the stratiform and convective areas thanks to the 5th and 95th percentiles of TWC and vertical wind speed. Hence, conditions of the stratiform area are TWC = [0.005, 0.75] g m^{-3} and w = [-4.5, 3] m s^{-1} while TWC = [0.02, 3] g m^{-3} and w = [-4, 4] m s^{-1} for convective regions.

Fig. 4 for the stratiform region is:

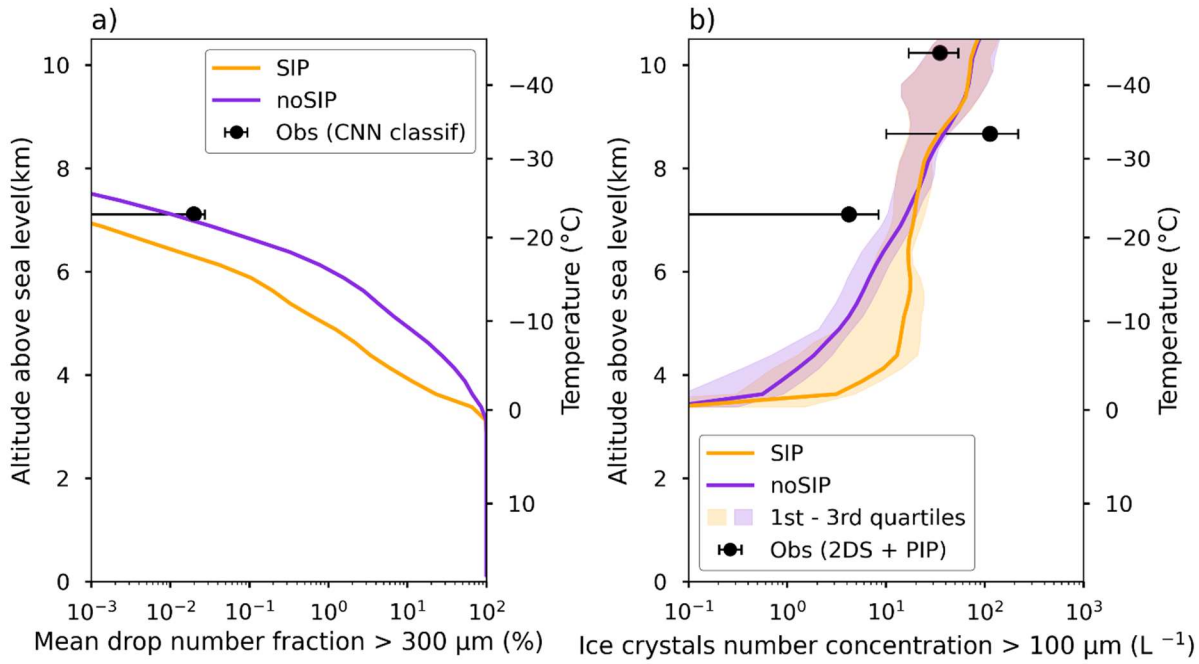

Figure 4 (stratiform region). a) Vertical mean profiles of the drop number fraction (> 300 µm) from the SIP and noSIP simulations at 08:20 UTC compare with the fraction derived from the CNN classification. b) Vertical mean profiles of ice

crystal number concentration (Nice) for particles larger than 100 µm from both simulations and 2DS and PIP probes measurements. Error bars and shaded areas indicate the 1st and 3rd quartiles.

Fig. 4 for the convective region is :

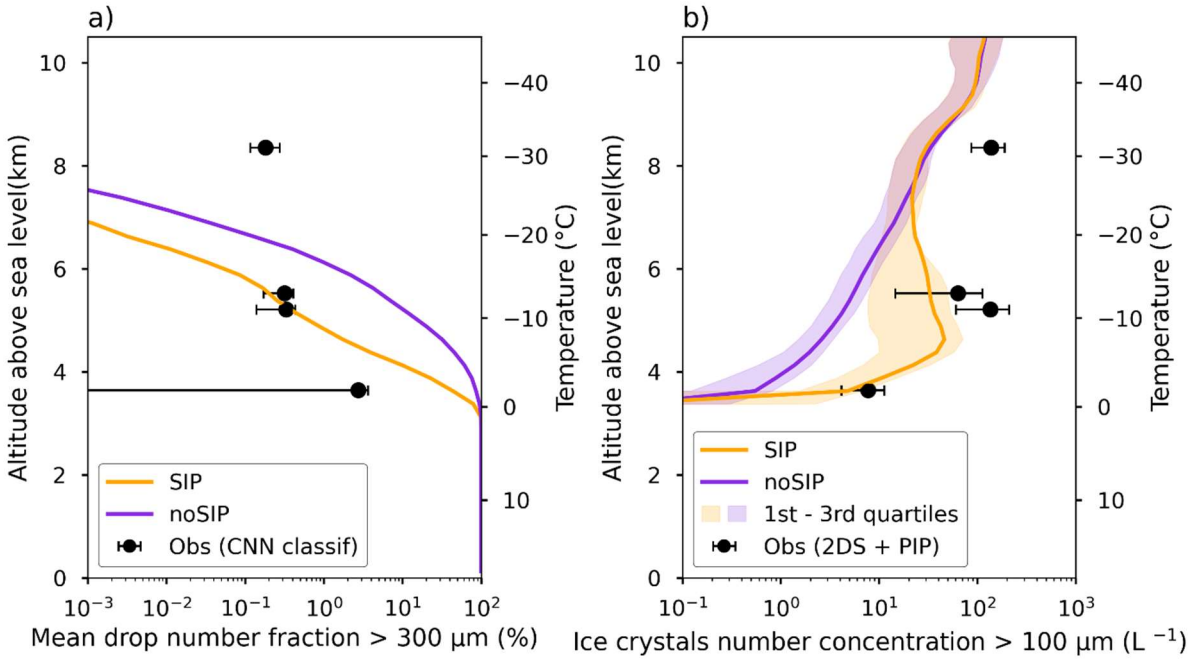

Figure 4 (convective region). a) Vertical mean profiles of the drop number fraction (> 300 µm) from the SIP and noSIP simulations at 08:20 UTC compare with the fraction derived from the CNN classification. b) Vertical mean profiles of ice crystal number concentration (Nice) for particles larger than 100 µm from both simulations and 2DS and PIP probes measurements. Error bars and shaded areas indicate the 1st and 3rd quartiles.

When comparing these two figures to the original Fig. 4 with the global TWC and w conditions, the differences are quite minor especially the ice particle number concentration comparison in Fig 4. b. The only visible difference is for the stratiform regions, where the drop number fraction obtain below -20°C is lower than for the convective region. However, the convective regions only show one point at this altitude which is not so robust. Indeed, the main problem of separating this plot into specific regions is that we have a limited number of legs and therefore datapoints. We think that this categorization for modeling and aircraft observation would be more suitable for larger observational datasets. We therefore prefer to keep the original version of Fig. 4, which conveys a similar message as a separation of Fig. 4 in convective and stratiform regions. However, we understand that it is relevant to separate the dataset in different regions to study cloud variability.

Furthermore, since we saw some differences of drop fractions regarding the convection and stratiform region, we modify and added some clarification (see line 214 or line 224 of diff pdf) for the description of Fig. 4a: *"For T <- 20°C, it is important to note that in two cases (at 8.5 km and 10 km), the observed drop fraction is zero, and that these points are therefore not*

represented in Fig. 4a. Three of the four drop fraction points observed at T < -20°C (two zeros and a 0.02% value at 7.5 km) correspond to stratiform conditions (i.e. before 8:15 UTC) while the fourth and highest drop fraction at this level (0.2% at 9 km) corresponds to convective conditions after 8:15 UTC. This highlights that the drop fraction at this altitude is highly dependent on the environmental conditions. However, with only four data points that vary significantly, it remains difficult to determine which simulation better matches the observations near the cloud top. Additional observations are needed to better evaluate the liquid and ice partitioning in DESCAM depending on environmental factors such as the convective and stratiform cloud regions observed after and before 08:15 UTC."

L205-206: Need more justifications here. How about the number of drops with sizes between 100 and 300 microns?

We found that the mean drop fraction for particles > 100 µm is only about a factor of 10 higher than that for particles > 300 µm. This suggests that even if selecting observations for particles > 100 µm may include more drops, their number remains significantly lower than that of ice particles. Therefore, the sentence in lines 205–206 has been updated (see line 224 or line 235 of diff pdf) with: "*Since the mean observed drop fraction for > 300 µm particles presented in Fig. 4a reaches only a maximum of 3% next to the melting layer (3.5 km), and that the modeled drop fraction > 100 µm at this level (not shown here) is only about one order of magnitude higher than that for particles > 300 µm, we assume that all particles larger than 100 µm detected by the 2DS and PIP probes as ice crystals. Therefore, we consider these measurements as comparable to Nice (> 300 µm) in DESCAM. This hypothesis is also commonly used when comparing model results to in situ aircraft measurements with for example, for > 75 µm particles in Arteaga et al. (2024), or even > 50 µm particles in Grzegorczyk et al. (2025a). This assumption can be further confirmed when looking at the 2DS + PIP and CDP measurements presented in Fig. 6 depicting the rise of particle number from 100 µm up to a 300 µm which probably corresponds to the deposition growth mode of ice particles.".*

L277-278: as mentioned previously, another factor of changed connectiveness for deep convective cases should be discussed as well.

Sorry but we don't understand what you mean by "changed connectiveness for deep convective".

L293-294: For the selection of the model grid, in addition to the similar altitude within ±150m, are the distance to these two stations considered?

No, we did not consider the distance from these two stations to select the model points as the precipitation is lacking at the south of the domain and does not even cover StEF station.

Therefore, we focused on the rain properties at grid points of similar altitude and rainfall intensity, within the dashed red line area presented in Fig. 1b. To ensure that our methodology is clear, we modify sentence L293-294 (see line 319 or line 329) with *"Consequently, to perform the comparison, we selected model grid points at the surface within the area presented in Fig. 1b, whose elevations were close (within ± 150 m) to those of the distrometers."*. As mentioned previously for the aircraft measurements, this method has the advantage of considering a larger number of grid points and thus improving the statistical significance of the mean modeled DSD.

L391-393: Good to have this statement as the SIP parameterizations are largely uncertain, even for the Hallett-Mossop process!!

Thank you !

Other comments:

L1: "cloud mixed phase" à mixed-phase cloud.

Corrected

L4, L6, L39: please add explanation of the acronyms: IOP7a, HYMEX, DESCAM.

The three acronyms are now detailed in L4 and L9 but there is no "DESCAM" written in line 38, and DESCAM acronym was already detailed in line 39.

L59: "the HYMEX-IOP7a heavy precipitation event" à the HYMEX-IOP7a is a heavy precipitation event"

Sorry, we don't understand what was wrong here.

L69: The HYMEX program (HYdrological Cycle in the Mediterranean EXperiment), HYMEX was already explained previously.

The text in parenthesis has been removed.

L84: the ARAMIS not explained.

Done

Fig 1: I believe adding some satellite images might help to understand the weather condition for this case study.

This is a satellite image (at 8h12 UTC 26-09-2012) from geostationary satellite Meteosat (SERVI radiometer sensor). Blue colors indicate the presence of ice phase clouds and white indicate liquid clouds.

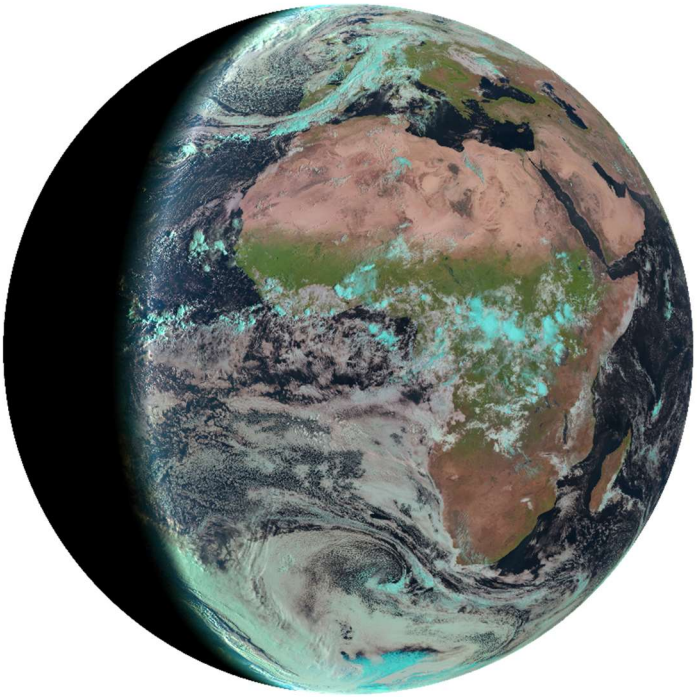

This is a focus on the Mediterranean region (8h12 UTC 26-09-2012)

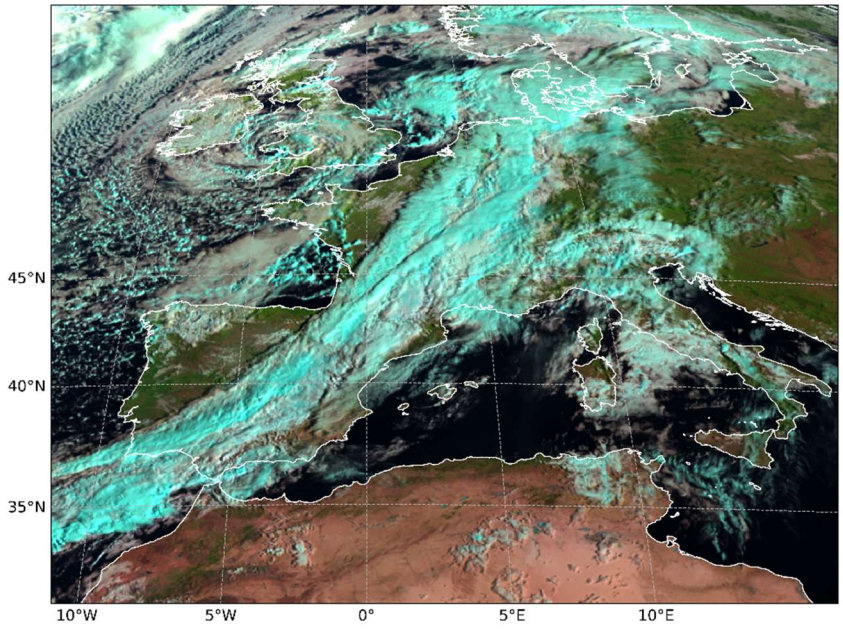

This is clear that there is an influence from the Spain region. However, we think that it does not bring any additional information that could significantly improve the paper and the understanding of the situation of the case.

L150: “The simulations are performed on Sept. 26, 2012” à “The simulations are performed for Sept. 26, 2012”? I guess this is the date of the flight, not the date when the simulation was run.

Yes this is true, we modified this sentence by “*The simulations are performed for the IOP7a case observed on Sept. 26, 2012, from 00 UTC to 12 UTC with a time step of Δt = 2s”*

L161: “Fig. 1b” à “Fig. 2b”?

Yes, this is corrected, thank you.

L264: “at the south of the two domain” à “at the south of the two stations”?

Yes, thanks for spotting the mistake.

Reviewer #2:

The manuscript titled "Influence of Secondary Ice Production on cloud and rain properties: Analysis of the HYMEX IOP7a Heavy Precipitation Event" presents a thorough numerical modelling study assessing the impact of Secondary Ice Production (SIP) on cloud microphysics and precipitation during a specific heavy rainfall event (HYMEX IOP7a). It builds on prior modelling efforts and extends them by incorporating SIP parameterisations into the DESCAM bin microphysics model. The manuscript is generally well-structured, and the methods and results are clearly presented. The authors make effective use of both airborne and ground-based observations for model validation.

The paper shows that modelled SIP processes substantially increase ice crystal number concentrations and shift the ice mass toward smaller hydrometeors. The associated reduction in total and heavy precipitation, as well as the shift in particle size distributions, are valuable outcomes for modellers and parameterisation developers.

My main concern is that I would like to see a more detailed explanation of how the SIP mechanisms were implemented in the model. Currently, these details are limited to Section 3.1 (lines 138–144).

In the referenced paper of Grzegorczyk et al. 2025a (https://doi.org/10.1016/j.atmosres.2024.107774) all three SIP processes as well as their implementation in context with our microphysics scheme were described. We therefore voluntarily shortly mention these implementations as the purpose of the present paper is focused on the effect of SIP on both cloud and precipitation properties. However, as the SIP description in Grzegorczyk et al. 2025a also encompasses several other SIP parametrizations, we added three

Appendices A1-A3 (available at the end of the document) which recap the implementation of the three SIP schemes in question. In addition, the content of Section 3.1 was modified to describe with more details about our microphysics scheme and the SIP mechanisms included as follows:

"3.1 Numerical experiment

Simulations of this study are performed using DESCAM bin microphysics scheme (Flossmann and Wobrock, 2010) implemented in the 3D dynamical model of Clark et al. (1996) and Clark (2003). DESCAM encompasses size distributions for the number of aerosol particles, cloud droplets and ice particles, with 39 bins each. Two further size distributions give the aerosol mass inside each droplet and each ice crystal bin. Another distribution function describes rime mass included in each ice particles and restricts to 27 bins (i.e. > 32 µm ice particles). The evolution of all 222 bins is determined by individual budget equations respecting transport processes (advection, turbulence, and sedimentation) as well source and sink terms given by cloud microphysics. The microphysics processes included in DESCAM are drop nucleation, deactivation, condensation, collision-coalescence, as well as heterogeneous and homogeneous ice nucleation, ice deactivation, vapor deposition growth, riming and aggregation. Three SIP processes were recently implemented into DESCAM (see Grzegorczyk et al., 2025a, b). Although the SIP parameterizations and implementation in DESCAM are detailed in Grzegorczyk et al. (2025a), a brief summary is given hereafter and more are available in Appendix A.

The first SIP process considered in DESCAM is the Hallett-Mossop process (HM) which is activated between -3°C to -8°C. It is temperature dependent within this temperature range, reaching a maximum of 350 fragments per mg of rime produced at -5°C (Hallett and Mossop, 1974). This temperature dependency is based on Eq. 72 of Cotton et al. (1986). More details about HM are presented in Section A1 of Appendix A.

The second process implemented in DESCAM is drop shattering during freezing (DS), parameterized following Phillips et al. (2018). It includes two modes: mode 1, which occurs during collisions between droplets with smaller ice crystals or through heterogeneous freezing, and mode 2, which occurs when raindrops are accreted by more massive ice particles. The equations taken from Phillips et al. (2018) used in DESCAM are presented in Section A2 of Appendix A.

Finally, fragmentation due to ice-ice collisions (BRK) is based on Phillips et al. (2017b) formulation but with parameters derived from the laboratory study of Grzegorczyk et al. (2023) for graupel or snow aggregate fragmentation experiments. Since DESCAM does not categorize ice particles but predicts their rime mass, the breakup of ice particles with less

than 50% rime mass follows snow aggregate behavior, while those above 50% follow graupel behavior. A full description of the BRK parameterization in DESCAM is given in Section A3 of Appendix A.

In DESCAM, SIP is also determined by the collision rates of hydrometeors, which requires to solve the stochastic collision equations for ice-droplet collisions (for HM and DS) and ice-ice collisions (for BRK), following the method of Bott (1998).”

While the relevant papers are cited, some of them—particularly Phillips et al. (2018)—include multiple options and parameterisation pathways. For instance, that paper provides several approaches, including equations 43–45 (empirical estimates), equation 15 (physics-based formulation), and equations 6 and 7 (collision-based framework for ice–liquid interactions). It is not clear which of these were used in DESCAM.

DESCAM applies a straightforward solution for collision, collection, and break-up of all types of hydrometeors. Thus, equations 43-45 are not relevant in our model. The equations 1 to 7 from Phillips et al. (2018) are applied and described in Appendix A2. In the initial version of the paper we mention *“The second is drop shattering during freezing (DS), following mode 1 and mode 2 of Phillips et al. (2018) parameterization”.* The ‘mode 1’ and ‘mode 2’ are clearly presented in two separate sections 4.1 and 4.2 in Phillips et al. (2018).

To be sure to avoid any confusion, we replace this sentence (see line 148 or line 152 of diff pdf) by “*The second process implemented in DESCAM is drop shattering during freezing (DS), parameterized following Phillips et al. (2018). It includes two modes: mode 1, which occurs during collisions between droplets with smaller ice crystals or through heterogeneous freezing, and mode 2, which occurs when raindrops are accreted by more massive ice particles. The equations taken from Phillips et al. (2018) used in DESCAM are presented in Section A2 of Appendix A.”*.

Similarly, for ice–ice collisional breakup, Phillips provides different formulations depending on the interacting ice types (e.g., graupel, snow, hail) and their temperature regimes. Was this complexity implemented? If so, how was it handled in DESCAM?

Yes Phillips et al. 2017 provides different parameters depending on the type of ice particle. However, as we mentioned, *“Finally, fragmentation due to ice-ice collisions (BRK) is based on Phillips et al. (2017b) formulation but with parameters derived from the laboratory study of Grzegorczyk et al. (2023).”* which means that Phillips et al. 2017 formulation is used but we but parameters from the laboratory results of Grzegorczyk et al. (2023) were employed for this formulation.

To clarify that we update the previous sentence (see line 152 or line 157 of diff pdf) to “*Finally, fragmentation due to ice-ice collisions (BRK) is based on Phillips et al. (2017b) formulation*

but with parameters derived from the laboratory study of Grzegorczyk et al. (2023) for graupel or snow aggregate fragmentation experiments. Since DESCAM does not categorize ice particles but predicts their rime mass, the breakup of ice particles with less than 50% rime mass follows snow aggregate behavior, while those above 50% follow graupel behavior. A full description of the BRK parameterization in DESCAM is given in Section A3 of Appendix A.". Furthermore, details about the ice-ice breakup parameterization along with equations are included in DESCAM in Appendix A3.

Additionally, the description of the Hallett-Mossop parameterization was also improved in section 3.1 (see line 144 or line 148 of diff pdf) with *"The first SIP process considered in DESCAM is the Hallett-Mossop process (HM) which is activated between -3° C to -8°C. It is temperature dependent within this temperature range, reaching a maximum of 350 fragments per mg of rime produced at -5°C (Hallett and Mossop, 1974). This temperature dependency is based on Eq. 72 of Cotton et al. (1986). More details about HM are presented in Section A1 of Appendix A."* as well as detailed equations presented in Appendix A1

In summary, I believe the paper would benefit significantly from a more transparent and detailed description of how these SIP parameterisations were implemented. This is a central part of the study, and readers will need this information to assess, reproduce, or build upon the work.

With the updated section 3.1 and the three sections describing SIP in appendix, we hope that it substantially improves the quality of the paper.

I have therefore suggested a Major Revision, although the necessary changes may turn out to be relatively minor if the authors can clearly describe the current implementation.

Appendix A

Parameterization of secondary ice production in DESCAM

A.1 Hallett-Mossop (HM)

The number of ice fragments generated by the Hallett-Mossop process in DESCAM is defined by:

$$\frac{\partial n_I(m_{frag})}{\partial t} = N_{HM} \cdot fct(T) \cdot \left(\frac{\partial m_r(m)}{\partial t} \right) \tag{A.1}$$

with n_I the number of ice particles, m_{frag} the fragments mass, $m_r(m)$ the newly accreted rime mass from droplets larger than 24 µm in diameter and of mass m. $m_r(m)$ is calculated from the stochastic equation solution scheme of Bott (1998) which provides the mass gained by ice particles that accreted droplets (see Eq. 1 of Grzegorczyk et al., 2025). N_{HM} is the number of fragments produced at -5°C, which is set to 350 per mg^{-1} as found in Hallett and Mossop (1974). The temperature dependency function $fct(T)$ is coming from Eq. 72 of Cotton et al. (1986), based on the experiments of Hallett and Mossop (1974). $fct(T)$ is set to be equal to 1 at -5°C and to linearly decrease to 0 at -3°C and -8°C.

The mass of ice fragments m_{frag} is assumed to depend on the parent drop mass (based on the observations of Choularton et al., 1980) and is given by

$$m_{frag}(m) = \min \left(0.015 \times m, 1.71 \times 10^{-8} \right) \tag{A.2}$$

with m the mass of the accreted drop (in g).

A.2 Drop shattering during freezing (DS)

DESCAM considers drop shattering during freezing from two modes which are presented in Phillips et al. (2018). Mode 1 is activated in DESCAM when large drops collect less massive ice particles or during heterogeneous drop freezing. The number of drops that freeze upon collision with less or more massive ice particles is determined from the stochastic equation solution scheme of Bott (1998), while the number of droplets frozen by heterogeneous ice nucleation is calculated from the Hiron and Flossmann (2015) method which is implemented in DESCAM (see Eq. 4 of Grzegorczyk et al., 2025).

The total number of ice fragments for each frozen drop generated by mode 1 is given by

$$\frac{\partial n_I(m_{frag})}{\partial t} = N_{DS}(m,T) \cdot \left(\frac{\partial n_D(m)}{\partial t}\right)_{freez}. \tag{A.3}$$

m_{frag} is the mass of the fragments and $N_{DS}(m,T)$ is the total number of fragments for one frozen drop which is calculated from Eq. 1 of Phillips et al. (2018) as follow:

$$N_{DS,1} = F(D)\Omega(T)\left[\frac{\zeta\eta^2}{(T-T_0)^2+\eta^2} + \beta T\right]. \tag{A.4}$$

with T the drop temperature, D the drop diameter. The two thresholds $\Omega(T)$ and $F(D)$ are used to activate fragmentation smoothly from -3 to -6°C as well as from drops size of D = 50 to 60 µm. The parameters T_0, β, ζ and η that depend on drop size are fitted in Phillips et al. (2018) based on a wide laboratory experiment dataset.

Furthermore, from the total number of fragments (Eq. A.4), Phillips et al. (2018) distinguish small and large fragments. The small fragments are to be 10 µm in size, and their number is given by $N_{DS,1}^{small} = N_{DS,1} - N_{DS,1}^{big}$. The large fragments number $N_{DS,1}^{big}$ formed from 'mode 1' is:

$$N_{DS,1}^{big} = \min\left\{F(D)\Omega(T)\left[\frac{\zeta_B\eta_B^2}{(T-T_{B,0})^2+\eta_B^2} + \beta_B T\right], N_{DS,1}\right\}. \tag{A.5}$$

Parameters of Eq. A.5 for large fragments are representing the same quantities than the total number of fragments in Eq. A.4. The large fragments mass is set to be 1/2.5 times the mass of parent drop.

Mode 2 occurs during collision of drops with more massive ice particles. In Phillips et al. (2018) the number of ice fragments formed via mode 2 is expressed by

$$N_{DS,2} = 3\Phi \cdot \Big[1 - f(T)\Big] \cdot \max(DE - DE_{crit}, 0). \tag{A.6}$$

with $DE = \frac{K_0}{\sigma\pi D^2}$ is the dimensionless energy which is defined by the ratio between collision kinetic energy and the drop surface tension, $DE_{crit} = 0.2$ represents the threshold of DE for the onset of drop splashing, $f(T)$ is the frozen fraction of the drop which depends on temperature. Φ is the fraction of ice fragment regarding total number of fragments (liquid + ice). We consider that Φ=0.3 which is based on the experimental study of James et al. (2021). Furthermore, the mass of the fragments is set to be 1000 times smaller than the mass of the parent drop as indicated in Phillips et al. (2018).

A.3 Fragmentation due to ice-ice collisions (BRK)

In DESCAM, the rate at which ice particles collide without sticking and therefore may break is described by the stochastic breakup equation (Eq. 14 in Grzegorczyk et al., 2025) and is treated within the Bott (1998) scheme.

The number of fragments generated per collision, is based on the formulation of Phillips et al. (2017) but using the experimental results of Grzegorczyk et al. (2023) laboratory study. The number

of fragments of mass m'' produced from the fragmentation of ice particle of mass m due to the collision with m' is given by

$$N_{BRK}(m'';m',m) = N^{tot}_{BRK}(m,m') \cdot P(m,m''). \tag{A.7}$$

$P(m,m'')$ is the number density distribution that gives the probability to generate a fragment of mass m'' from the total number of fragments $N^{tot}_{BRK}(m,m')$ during the fragmentation of an ice particle of mass m. The total number of fragments is determined from Phillips et al. (2017) theory by:

$$N^{tot}_{BRK}(m,m') = \alpha(m,\phi)A_M(T,\phi)\left(1-\exp\left(-\frac{C(\phi)K_0(m,m',\phi,\phi')}{\alpha(m,\phi)A_M(T,\phi)}\right)^{\gamma}\right). \tag{A.8}$$

$\alpha(m,\phi)$ is the smallest area of the two colliding ice particles (in m^2), $A_M(T,\phi)$ is the number density of breakable asperities on ice particles per unit area (in m^{-2}), $C(\phi)$ is the asperity-fragility parameter (in J^{-1}), $K_0(m,m',\phi,\phi')$ is the collision kinetic energy (CKE), γ is a shape parameter, ϕ and ϕ' are the rime fractions of the colliding ice particles.

The $A_M(T,\phi)$, $C(\phi)$ and γ parameters are determined from Grzegorczyk et al. (2023) experimental results, for 3 collisions types. Results of graupel-snowflake collisions are employed for the breakup of ice particles with $\phi < 0.5$ while for $\phi > 0.5$ (i.e. rimed particles) graupel-graupel and graupel-graupel with dendrites results are used and interpolated as function of the supersaturation with respect to ice (S_i). We employ this supersaturation dependency as graupel-graupel collisions are performed in an environment without any vapor depositional (i.e. S_i supposed to be close to 0) whereas graupel-graupel with dendrites collisions are done in a high supersaturation environment ($S_i = 0.23$). The parameters of Eq. A.8 for -15°C are given in Table. A.1.

Rime fraction	$\boldsymbol{A_M(-15°\mathrm{C},\phi)}$ (m^{-2})	$\boldsymbol{C}$ (J^{-1})	$\boldsymbol{\gamma}$
$\phi < 0.5$	5×10^6	5.8×10^8	0.78
$\phi > 0.5$	$\exp(14.74 \times S_i + 14.28)$	$\exp(20.15 \times S_i + 13.78)$	$S_i + 0.55$

Table A.1: Parameters used in DESCAM (at -15°C) for the fragmentation due to ice–ice collisions parameterization of Phillips et al. (2017). These parameters are derived from three types of collision experiments performed in Grzegorczyk et al. (2023) laboratory study. For $\phi < 0.5$ parameters corresponding to graupel–snowflake collisions are used, and for $\phi > 0.5$ an interpolation between graupel–graupel and graupel–dendrite collisions parameters is done as a function of the ice supersaturation S_i.

For temperatures different than -15°C, a temperature dependency is considered for $A_M(T,\phi)$. It is based on Takahashi et al. (1995) study that investigated the effect of temperature on the number of fragments at a large CKE regime. From Takahashi et al. (1995) results, Phillips et al. (2017) proposed triangular temperature dependency which is used here and defined by:

$$A_M(T,\phi) = A_M(-15°\mathrm{C},\phi)\left(\frac{1}{3}+\max\left(0.,\frac{2}{3}-\frac{1}{9}\times\left|15.0+T\right|\right)\right) \tag{A.9}$$

with the temperature T in °C. Regarding the fragment properties, the fragment mass distribution $P(m,m'')$, derived from the fragment size distribution of Grzegorczyk et al. (2023), is used to distribute the fragments across the bins of DESCAM. It is defined by:

$$P(m,m'') = \frac{1}{\sigma(m,\phi)\sqrt{2\pi}} \cdot \exp\left(\frac{\ln(m'')-\mu(m,\phi)}{2\sigma(m,\phi)^2}\right)\Delta m \tag{A.10}$$

with Δm the width of mass bins. From Grzegorczyk et al. (2023) study, which provides two distinct fragment size distributions for parent particles of different sizes (10 mm snowflakes and 4 mm graupel), we hypothesize that both the mode $\mu(m,\phi)$ and standard deviation $\sigma(m,\phi)$ of the distribution depend on the size of the parent ice particle. We therefore employs a linear interpolation to adjust $\mu(m,\phi)$ and $\sigma(m,\phi)$ as function of parent ice particle size of mass m as follows:

$$\begin{cases} \mu(m,\phi) = \min\Big(3.95 \cdot D(m,\phi) - 15.4, -9.475\Big) \\ \sigma(m,\phi) = \min\Big(1.28 \cdot D(m,\phi) + 1.17, 3.09\Big) \end{cases} \tag{A.11}$$

where $D(m,\phi)$ is the parent particle size in cm.

Bibliography

Bott, A., 1998: A flux method for the numerical solution of the stochastic collection equation. *Journal of the Atmospheric Sciences*, **55 (13)**, 2284–2293, doi:10.1175/1520-0469(1998)055<2284:afmftn>2.0.co;2, URL https://doi.org/10.1175/1520-0469(1998)055<2284:afmftn>2.0.co;2.

Choularton, T. W., D. J. Griggs, B. Y. Humood, and J. Latham, 1980: Laboratory studies of riming, and its relation to ice splinter production. *Quarterly Journal of the Royal Meteorological Society*, **106 (448)**, 367–374, doi:10.1002/qj.49710644809, URL https://doi.org/10.1002/qj.49710644809.

Cotton, W. R., G. J. Tripoli, R. M. Rauber, and E. A. Mulvihill, 1986: Numerical simulation of the effects of varying ice crystal nucleation rates and aggregation processes on orographic snowfall. *Journal of Climate and Applied Meteorology*, **25 (11)**, 1658–1680, doi:10.1175/1520-0450(1986)025<1658:nsoteo>2.0.co;2, URL https://doi.org/10.1175/1520-0450(1986)025<1658:nsoteo>2.0.co;2.

Grzegorczyk, P., W. Wobrock, A. Canzi, L. Niquet, F. Tridon, and C. Planche, 2025: Investigating secondary ice production in a deep convective cloud with a 3d bin microphysics model: Part i - sensitivity study of microphysical processes representations. *Atmospheric Research*, **313**, 107 774, doi:10.1016/j.atmosres.2024.107774, URL http://dx.doi.org/10.1016/j.atmosres.2024.107774.

Grzegorczyk, P., S. Yadav, F. Zanger, A. Theis, S. K. Mitra, S. Borrmann, and M. Szakáll, 2023: Fragmentation of ice particles: laboratory experiments on graupel–graupel and graupel–snowflake collisions. *Atmospheric Chemistry and Physics*, **23 (20)**, 13 505–13 521, doi:10.5194/acp-23-13505-2023, URL https://acp.copernicus.org/articles/23/13505/2023/.

Hallett, J. and S. C. Mossop, 1974: Production of secondary ice particles during the riming process. *Nature*, **249 (5452)**, 26–28, doi:10.1038/249026a0, URL https://doi.org/10.1038/249026a0.

Hiron, T. and A. Flossmann, 2015: A study of the role of the parameterization of heterogeneous ice nucleation for the modeling of microphysics and precipitation of a convective cloud. *Journal of the Atmospheric Sciences*, **72 (9)**, 3322–3339.

James, R. L., V. T. J. Phillips, and P. J. Connolly, 2021: Secondary ice production during the break-up of freezing water drops on impact with ice particles. *Atmospheric Chemistry and Physics*, **21 (24)**, 18 519–18 530, doi:10.5194/acp-21-18519-2021, URL https://doi.org/10.5194/acp-21-18519-2021.

Phillips, V. T. J., S. Patade, J. Gutierrez, and A. Bansemer, 2018: Secondary ice production by fragmentation of freezing drops: Formulation and theory. *Journal of the Atmospheric Sciences*, **75 (9)**, 3031–3070, doi:10.1175/jas-d-17-0190.1, URL https://doi.org/10.1175/jas-d-17-0190.1.

Phillips, V. T. J., J.-I. Yano, and A. Khain, 2017: Ice Multiplication by Breakup in Ice–Ice Collisions. Part I: Theoretical Formulation. *Journal of the Atmospheric Sciences*, **74 (6)**, 1705–1719, doi: 10.1175/JAS-D-16-0224.1.

Takahashi, T., Y. Nagao, and Y. Kushiyama, 1995: Possible high ice particle production during graupel–graupel collisions. *Journal of the Atmospheric Sciences*, **52 (24)**, 4523–4527, doi:10.1175/1520-0469(1995)052<4523:phippd>2.0.co;2.